Supplementary material to:

Global sensitivity of aviation NO_x effects to the HNO_3-forming channel of the HO_2 + NO reaction

K. Gottschaldt, C. Voigt, P. Jöckel, M. Righi, R. Deckert and S. Dietmüller

June 22, 2012

Contents: pages

1. Comparison of simulated versus observational profiles of selected trace gases 2 - 11

2. Rate coefficient of $CH_4 + OH \rightarrow CH_3 + OH$ 12 - 14

References 15

1 Comparison of simulated versus observational profiles of selected trace gases

In this section [HNO_3], [NO_x], [HO_x] and [O_3] profiles from simulations BA, DA and WA are compared to observational profiles of Emmons et al. (2000). The observational profile data are composites for different regions and campaigns from near the year 2000, as listed in Table S1. The simulation data were sampled according to the observational region and time of year, but not at the exact location and time of the individual measurements that entered the observational composite data. Mean values were calculated from all model output steps in the given time range. Furthermore the observational profiles may have been compiled from different years than the simulation year 2001. The comparison is considered a climatological one. However, each simulation profile and each observational profile is based just on a few of days of data from a single year. Thus this comparison may only give an overall idea if the order of magnitude of the above trace gas mixing ratios is realistic in the simulations.

The observational data of Emmons et al. (2000) are limited to the altitude range below 11 km (Fig. S1). Thus differences between [HNO_3] profiles from simulations BA, DA and WA are generally small. Some model data are lower than the corresponding observations, some are higher. At least the extreme values do always overlap. HNO3 is subject to scavenging, which strongly depends on local events like convection and rain. Individual scavenging events differ between model and observations, and may print through due to the short sampling periods. Furthermore, the heterogeneous reaction $N_2O_5 + H_2O \rightarrow 2HNO_3$ is calculated on all aerosol surfaces, throughout the atmosphere. However, in the troposphere N_2O_5 is rather converted into aqueous-phase NO_3-, but not released as gaseous HNO_3 (Jöckel et al., 2010). On the other hand, NO_3^- is potentially interpreted as HNO_3 in measurements (Keene et al., 1998). Since HNO3_tot in Fig. 1 and in Fig. S1 contains only gaseous HNO_3 and NAT, errors concerning NO_3- may partially compensate. Considering the above uncertainties, the model data match the [HNO3] observations well.

[NO_x] observations are generally well reproduced by all simulations (Fig. S2). Measured and simulated values do always overlap, standard deviations do mostly. Some measurements are in better agreement with BA, others with DA or WA.

Standard deviations of simulated ozone mixing ratios overlap with almost all measurements (Fig. S3). Ozone observations are very well reproduced, and there is no clear bias in any of the simulations.

The significant impact of OH mixing ratios on [CO] is reflected in Fig. 4. The HNO_3-forming channel of HO_2 + NO (Reaction R2) shifts profiles of simulated [CO] from lower to higher values. CO mixing ratios are mostly lower than the observations for BA, but ok for WA.

All three simulations (BA, DA, WA) match the observations well. Neither the chemical regime without the HNO_3-forming channel of HO_2 + NO, nor the two regimes with it can be ruled out according to this analysis.

Table S1. Campaign composite profile data (Emmons et al., 2000) used for the comparison to simulations BA, DA and WA in Fig. S1 – S4. The simulations were sampled for the same date ranges and region bounds as listed in this table. However, the simulation year characterised by synoptic dynamics and emissions was always 2001.

Campaign composite	Time range	year	lon_{min}	lon_{max}	lat_{min}	lat_{max}
PEM-Tropics-A_DC8 , Fiji	15.08.-15.10.	1996	170	-170	-30	-10
PEM-Tropics-A_DC8, Easter-Is.	15.08.-15.10.	1996	-120	-100	-40	-20
PEM-Tropics-A_DC8, Tahiti	15.08.-15.10.	1996	-160	-130	10	0
PEM-Tropics-A_DC8, X-mas-Is.	15.08.-15.10.	1996	-160	-140	0	10
TOPSE-Apr_C130, Boulder	02.04.-30.04.	2000	-110	-90	37	47
TOPSE-Apr_C130, Churchill	02.04.-30.04.	2000	-110	-80	47	65
TOPSE-Apr_C130, Thule	02.04.-30.04.	2000	-110	-60	65	90
TOPSE-Feb_C130, Boulder	04.02.-27.02.	2000	-110	-90	37	47
TOPSE-Feb_C130, Churchill	04.02.-27.02.	2000	-110	-80	47	65
TOPSE-Feb_C130, Thule	04.02.-27.02.	2000	-110	-60	65	90
TOPSE-Mar_C130, Boulder	05.03.-26.03.	2000	-110	-90	37	47
TOPSE-Mar_C130, Churchill	05.03.-26.03.	2000	-110	-80	47	65
TOPSE-Mar_C130, Thule	05.03.-26.03.	2000	-110	-60	65	90
TOPSE-May_C130, Boulder	15.05-23.05.	2000	-110	-90	37	47
TOPSE-May_C130, Churchill	15.05-23.05.	2000	-110	-80	47	65
TOPSE-May_C130, Thule	15.05-23.05.	2000	-110	-60	65	90
TRACE-P_DC8, China	24.02.-10.04.	2001	110	130	10	30
TRACE-P_DC8, Guam	24.02.-10.04.	2001	140	150	10	20
TRACE-P_DC8, Hawaii	24.02.-10.04.	2001	-170	-150	10	30
TRACE-P_DC8, Japan	24.02.-10.04.	2001	130	150	20	40

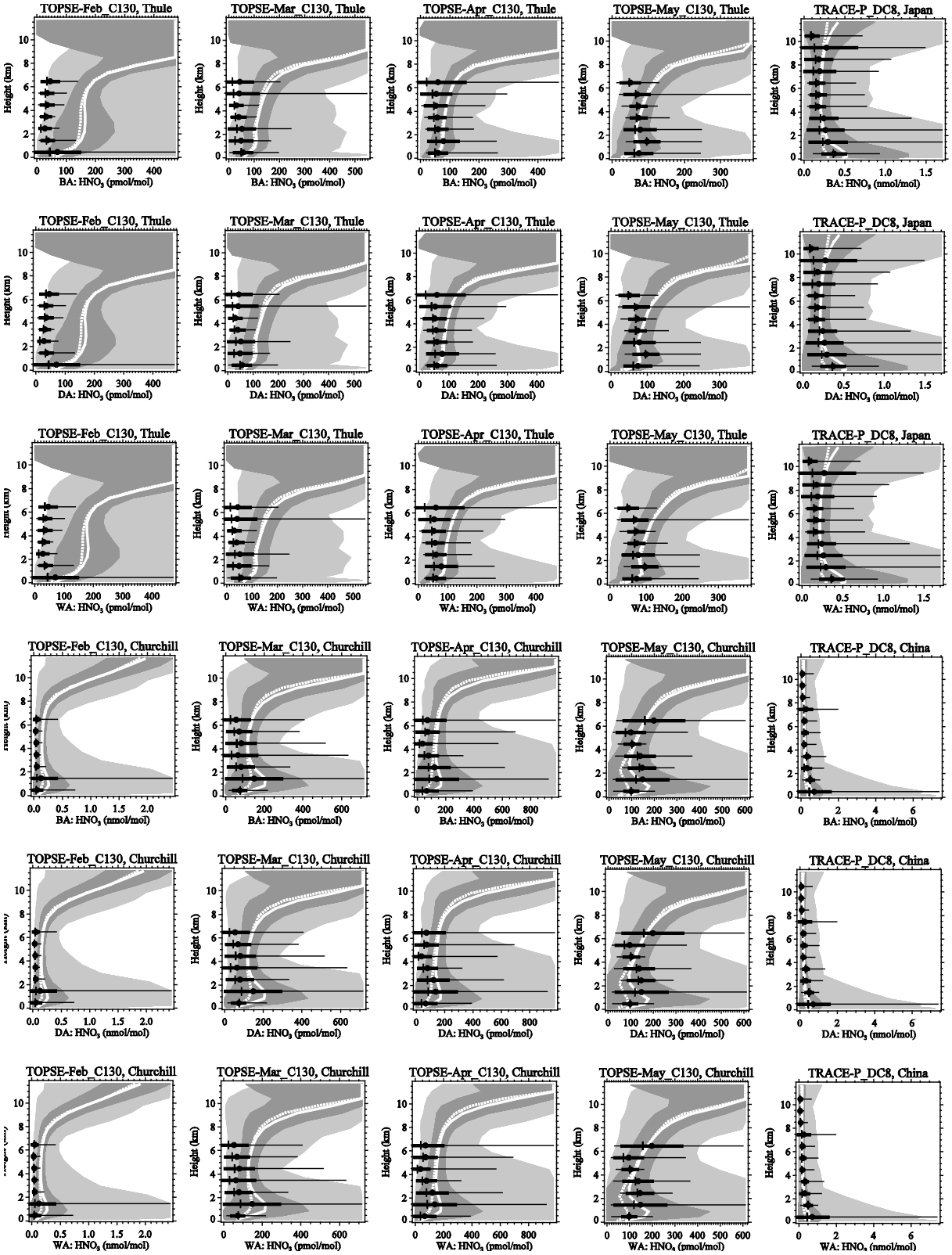

Figure S1a. Comparison of HNO_3 mixing ratio profiles as listed in Table S1. Black represents observational data: dot = mean, cross = median, thick error bar = standard deviation, thin error bar = range of values. Grey shading and white curves refer to simulations: solid line = mean, dotted line = median, dark grey = standard deviation, light grey = range of values (full range not always shown).

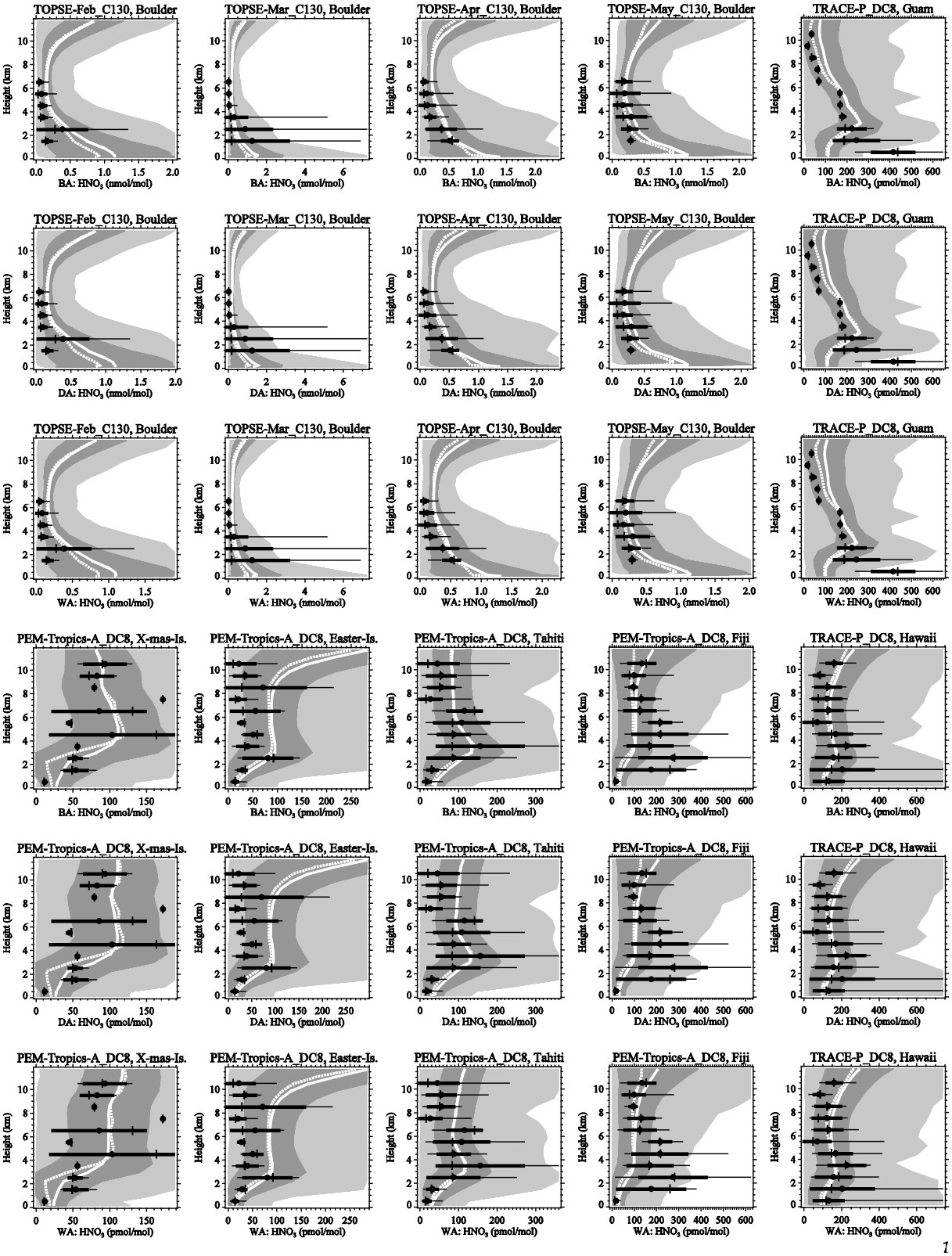

Figure S1b. Continued from Fig. S1a.

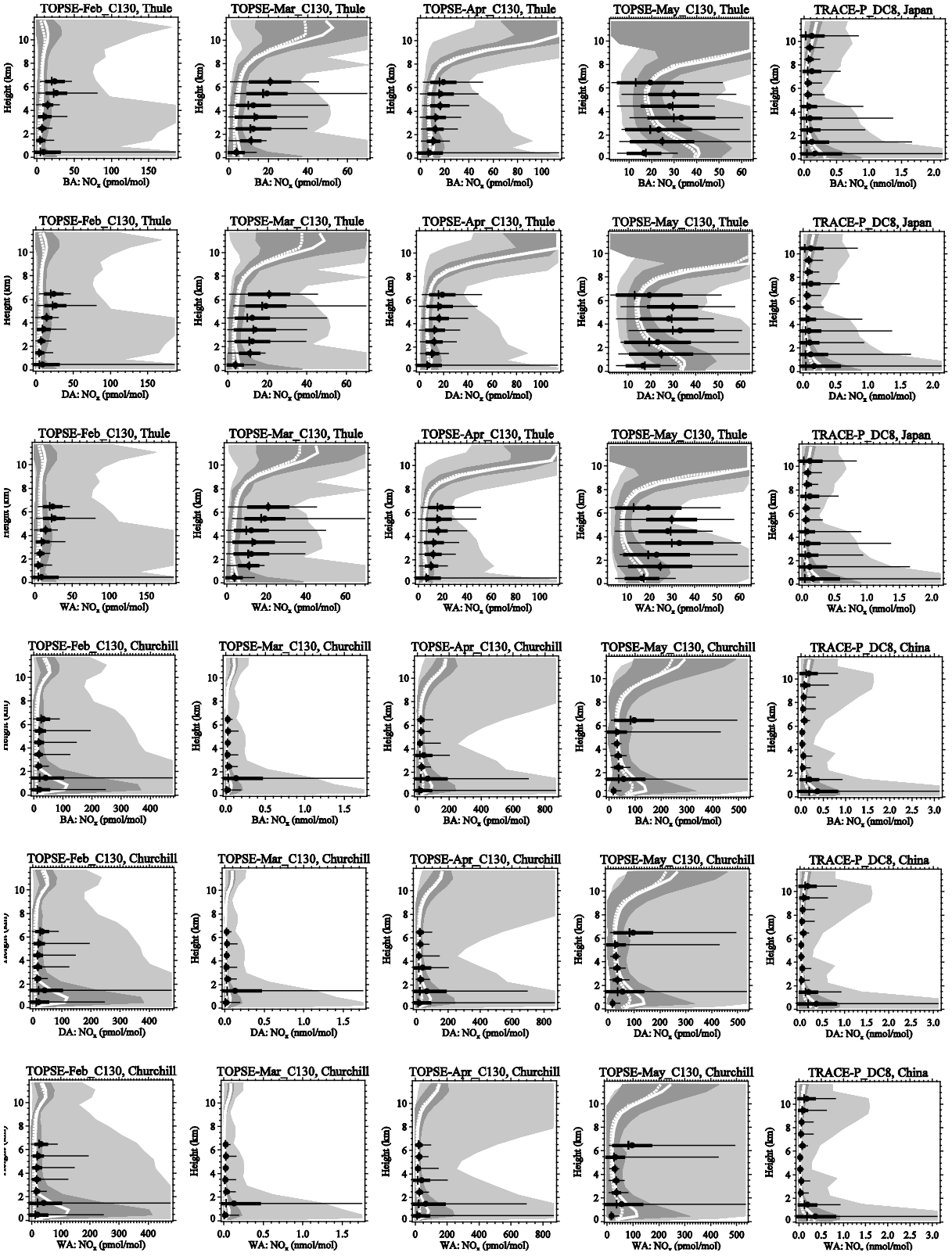

Figure S2a. As Fig. S1a, but for NO_x.

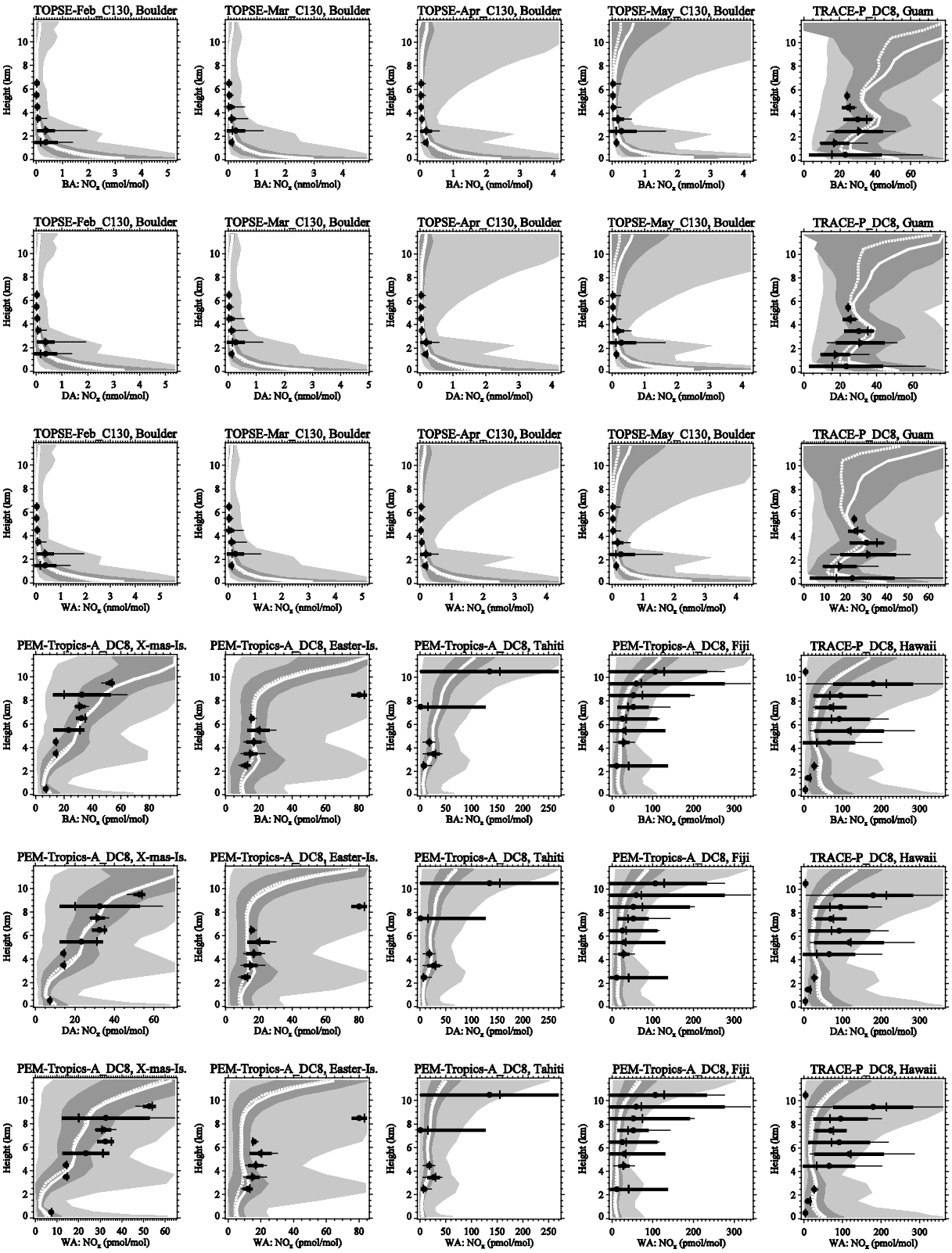

Figure S2b. Continued from Fig. S2a.

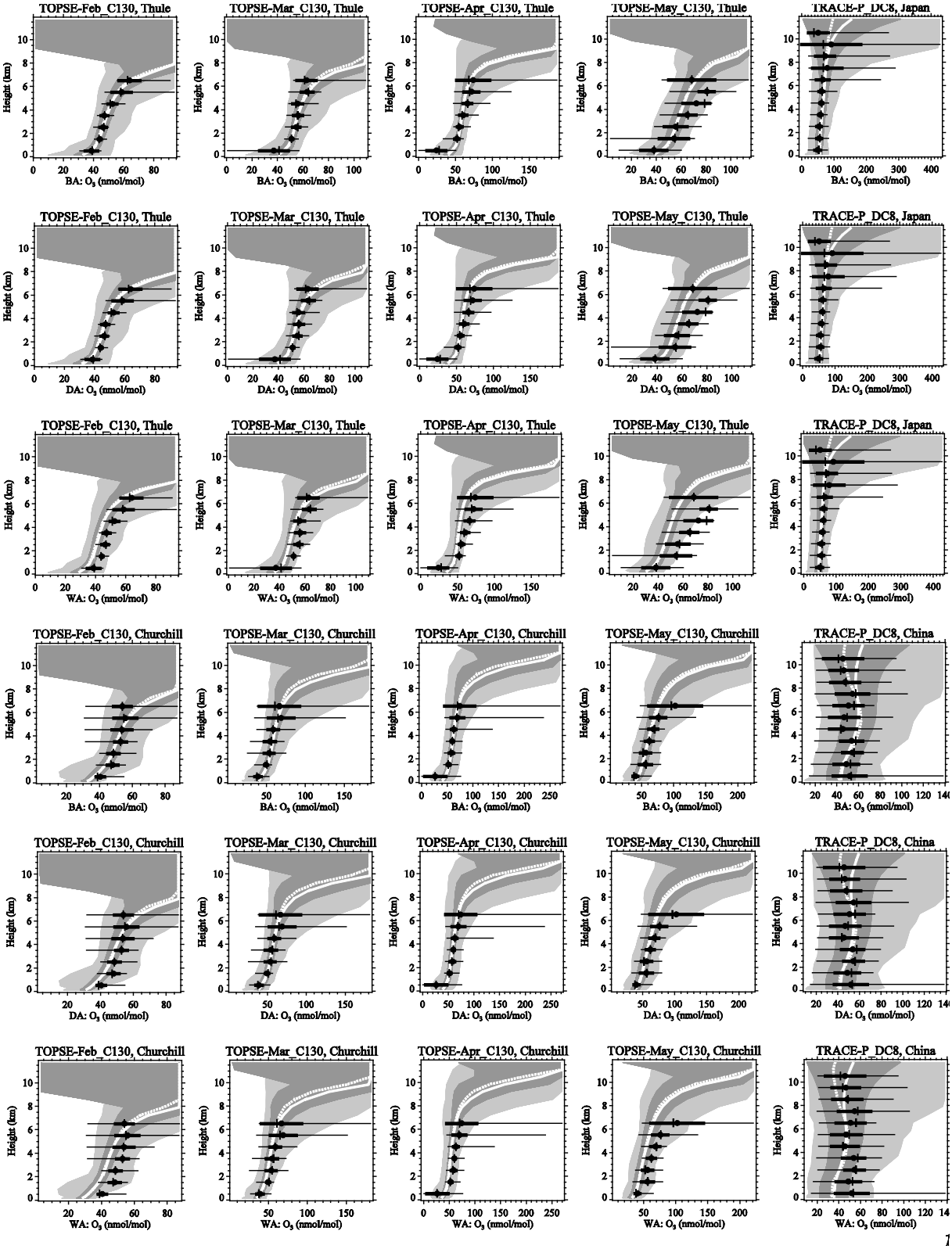

Figure S3a. As Fig. S1a, but for O_3.

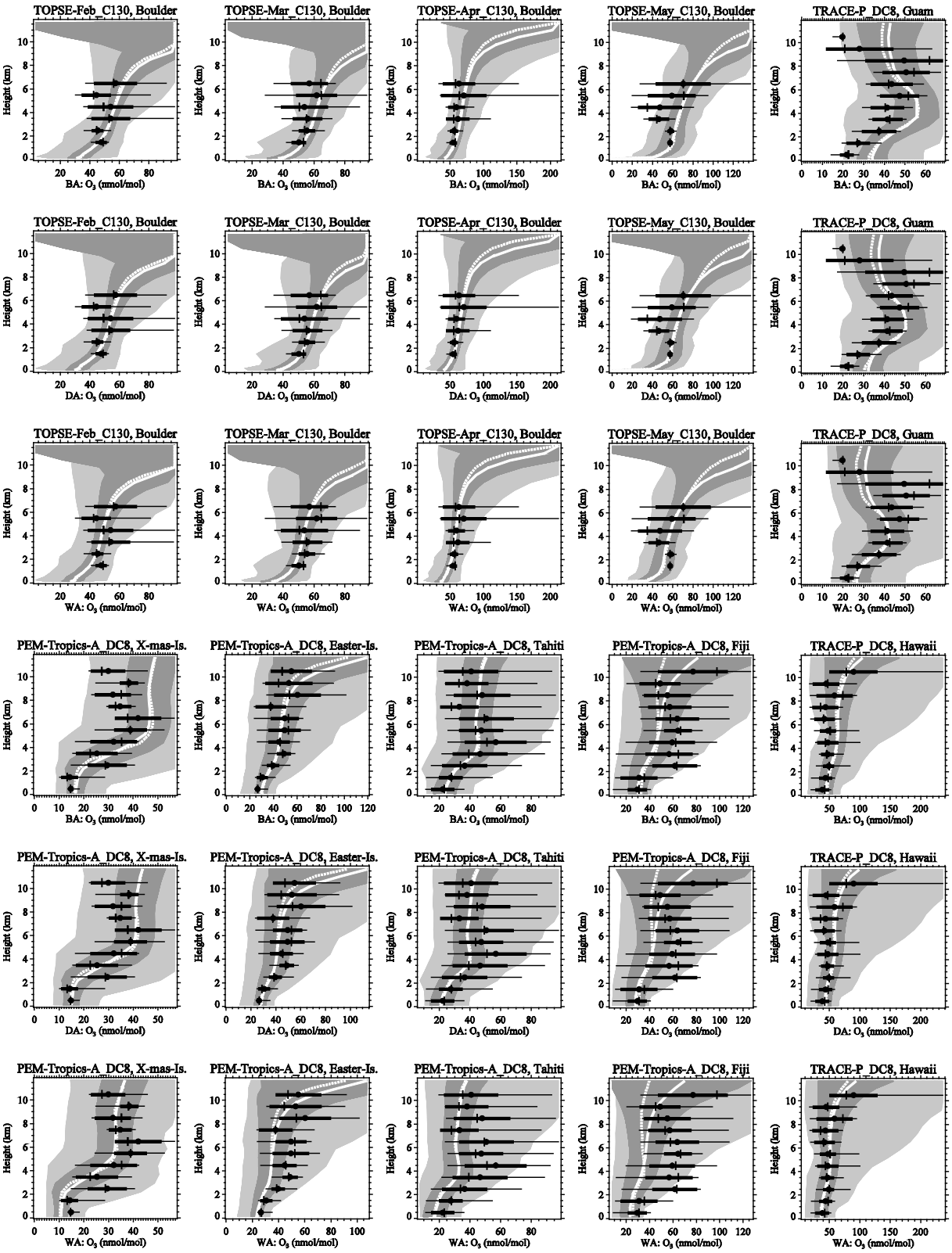

Figure S3b. Continued from Fig. S3a.

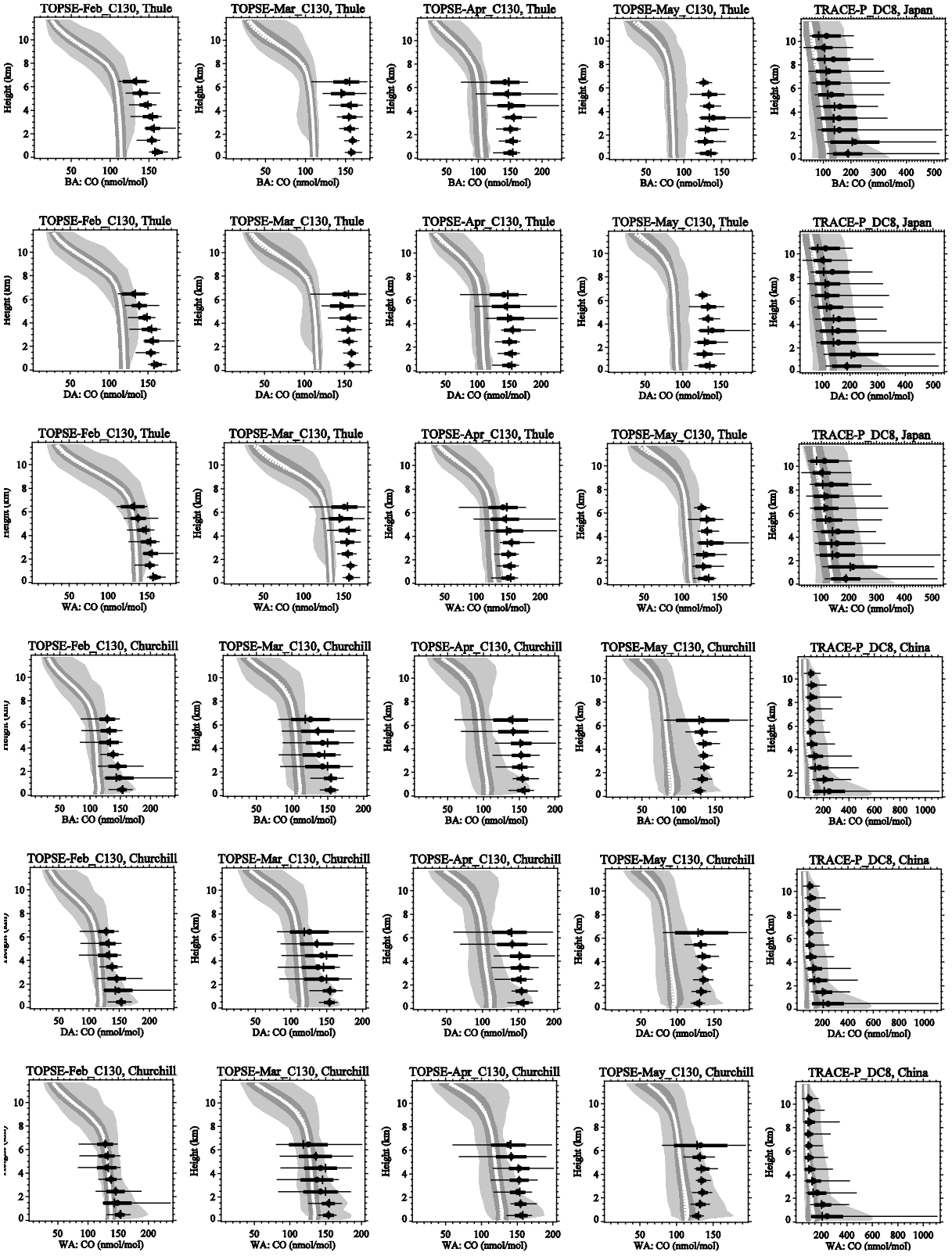

Figure S4a. As Fig. S1a, but for CO.

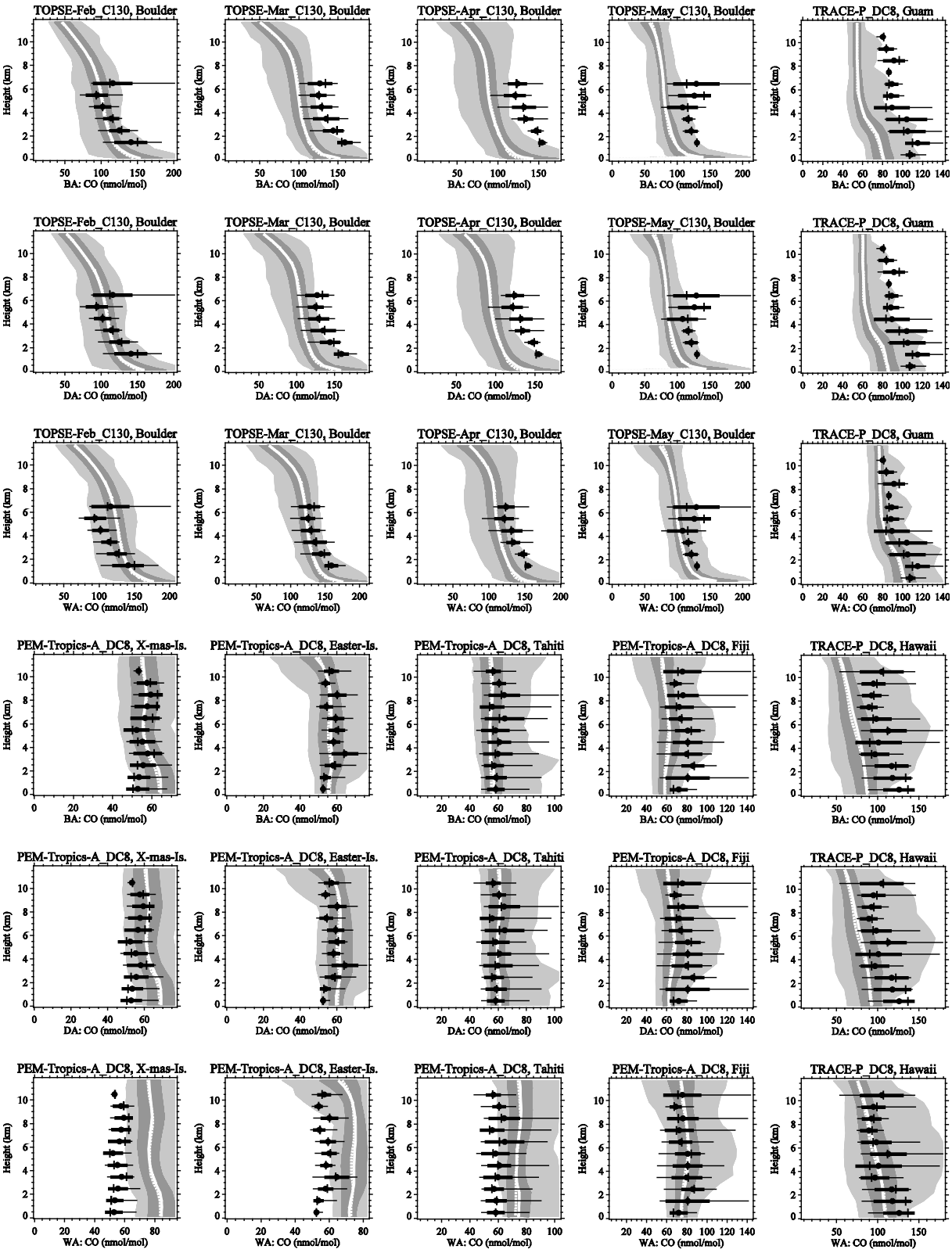

Figure S4b. Continued from Fig. S4a.

2 Rate coefficient of $CH_4 + OH \rightarrow CH_3 + OH$

Here we compare different formulations for the reaction rate coefficient k_{CH4} of CH_4 + OH $\rightarrow$ CH_3 + OH (Reaction R4), which has a significant impact on estimates of methane lifetime. All rate coefficients are given in $cm^3s^{-1}molecule^{-1}$ in the following. The rate coefficients proposed by Gierczak et al. (1997), Atkinson et al. (2003), IUPAC (2007) and Sander et al. (2011) all depend just on temperature. Some studies also provide a value of the rate coefficient at 298 K, which may have a different uncertainty range than formulations with temperature as a parameter would yield at 298 K.

IUPAC (2007) recommends for the temperature (T) range 200 K to 300 K:

$$k_{CH4}^{best,min,max} = 1.85 \cdot 10^{-12} \exp\left(\frac{-1690 \pm 100}{T}\right) \quad \text{(S1)}$$

The above formulation has been derived from the more accurate formulation of Gierczak et al. (1997), which is valid for the temperature range 195 K to 296 K:

$$k_{CH4}^{best,min,max} = 1.85 \cdot 10^{-20} \cdot T^{2.82} \exp\left(\frac{-987 \pm 6}{T}\right) \quad \text{(S2)}$$

This formulation is also recommended by Atkinson et al. (2003), which is used in this study. The uncertainty at 298 K is estimated to be ±20 % (Atkinson, 2003), which is different to the uncertainties given by Gierczak et al. (1997). Sander et al. (2011) recommend

$$k_{CH4}^{best} = 2.45 \cdot 10^{-12} \exp\left(\frac{-1775}{T}\right) \quad \text{(S3a)}$$

for 195 K to 300 K, with the uncertainty range

$$k_{CH4}^{min,max} = k_{CH4}^{best} \cdot \left\{1.1 \cdot \exp\left|100. \cdot \left(\frac{1}{T} - \frac{1}{298}\right)\right|\right\}^{\pm 1} \quad \text{(S3b)}$$

Uncertainty ranges at 298 K are summarized in Table S2. The temperature dependent formulations (Eq. S1, S2, S3) are plotted in Fig. S5. Their impact on methane lifetime and global mean OH concentration in simulations BA, DA, WA is summarized in Table S3. The recommended temperature dependent rate coefficients (k_{CH4}^{best}) of the different studies agree remarkably well (Fig. S5). Thus differences between τ_{CH4}^{OH} are likely to be small between

different modelling studies that used one of the above formulations for k_{CH4}^{best}. The full uncertainty of k_{CH4} needs to be considered though, when comparing τ_{CH4}^{OH} from studies that depend on k_{CH4} to others that do not.

Table S2. Comparison of reaction rate coefficients for CH_4 + OH → CH_3 + OH at 298 K, all in 10^{-15} cm^3/s/molecule.

Reference	$k_{CH4}^{min}(298\,K)$	$k_{CH4}^{best}(298\,K)$	$k_{CH4}^{max}(298\,K)$
IUPAC (2007) via Eq. S1	4.56	6.38	8.92
IUPAC (2007) at 298 K	5.32	6.40	7.69
Gierczak et al. (1997) via Eq. S2	6.28	6.40	6.54
Gierczak et al. (1997) at 298 K	6.02	6.40	6.78
Atkinson et al. (2003) via Eq. S2, ±20 %	5.34	6.40	7.69
Sander et al. (2011) via Eq. S3	5.77	6.35	6.99
Sander et al. (2011) at 298 K	5.73	6.30	6.93

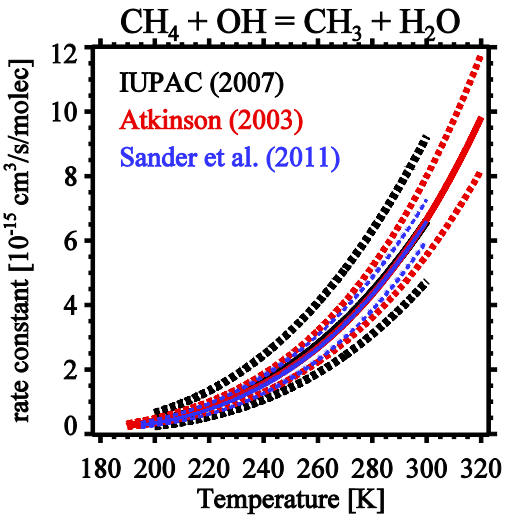

Figure S5. Temperature dependence of the reaction rate coefficient for CH_4 + OH → CH_3 + OH from different studies. Solid curves show the recommended values, dotted lines the corresponding uncertainty ranges.

Table S3. Comparison of methane lifetime and global mean OH concentration for the domain below the climatological tropopause from Eq. 8, and for the domain below 100 hPa (in brackets). τ_{CH4}^{OH} is given in years, $\langle c_{OH} \rangle$ in 10^6 cm^{-3}. Minimum (min), best and maximum (max) values reflect the uncertainty ranges of the rate coefficient for $CH_4 + OH \rightarrow CH_3 + OH$, as given by Eq. S1, S2 and S3. Note that the uncertainty given by Eq. S3b is a factor. It occurs in numerator and denominator of the weighting and thus has no effect on $\langle c_{OH}^k \rangle$.

	BA			DA			WA		
	min	best	max	min	best	max	min	best	max
τ_{CH4}^{OH} (IUPAC, 2007)	(5.5)	(7.9)	(11.4)	(6.1)	(8.7)	(12.6)	(8.2)	(11.8)	(17.0)
	5.2	7.5	10.8	5.7	8.3	11.9	7.8	11.2	16.1
τ_{CH4}^{OH} (Atkinson, 2003)	(6.7)	(8.1)	(9.7)	(7.4)	(8.9)	(10.7)	(10.0)	(12.0)	(14.4)
	6.3	7.6	9.1	7.0	8.4	10.1	9.5	11.4	13.7
τ_{CH4}^{OH} (Sander et al., 2011)	(7.2)	(8.2)	(9.2)	(8.0)	(9.0)	(10.2)	(10.7)	(12.2)	(13.8)
	6.8	7.7	8.7	7.5	8.5	9.6	10.2	11.5	13.0
$\langle c_{OH}^{mass} \rangle$		(1.22)			(1.09)			(0.823)	
		1.27			1.13			0.850	
$\langle c_{OH}^k \rangle$ (IUPAC, 2007)	(1.39)	(1.40)	(1.41)	(1.26)	(1.27)	(1.28)	(0.935)	(0.942)	(0.949)
	1.41	1.41	1.42	1.27	1.28	1.29	0.943	0.950	0.956
$\langle c_{OH}^k \rangle$ (Atkinson, 2003)	(1.40)	(1.40)	(1.40)	(1.27)	(1.27)	(1.27)	(0.945)	(0.945)	(0.945)
	1.42	1.42	1.42	1.29	1.29	1.29	0.953	0.953	0.953
$\langle c_{OH}^k \rangle$ (Sander et al., 2011)	(1.40)	(1.41)	(1.42)	(1.27)	(1.28)	(1.29)	(0.941)	(0.948)	(0.955)
	1.41	1.42	1.43	1.28	1.29	1.30	0.949	0.955	0.961

References

Atkinson, R.: Kinetics of the gas-phase reactions of OH radicals with alkanes and cycloalkanes, Atmos. Chem. Phys., 3, 2233–2307, 2003.

Atkinson, R., Baulch, D. L., Cox, R. A., Crowley, J. N., Hampson, R. F., Hynes, R. G., Jenkin, M. E., Rossi, M. J., and Troe, J.: Evaluated kinetic and photochemical data for atmospheric chemistry: Volume I - gas phase reactions of O_x, HO_x, NO_x and SO_x species, Atmos. Chem. Phys., 4, 1461-1738, doi:10.5194/acp-4-1461-2004, 2004.

Emmons, L. K., Hauglustaine, D. A., Müller, J.-F., Carroll, M. A., Brasseur, G. P., Brunner, D., Staehelin, J., Thouret, V., and Marenco, A.: Data composites of airborne observation of tropospheric ozone and its precursor, J. Geophys. Res., 105, 20 497–20 538, 2000. Data downloaded from http://acd.ucar.edu/~emmons/DATACOMP/camp_table.htm.

Gierczak, T., Talukdar, R. K., Herndon, S. C., Vaghjiani, G. L., and Ravinshankara, A. R.: Rate Coefficients for the Reactions of Hydroxyl Radicals with Methane and Deuterated Methanes, J. Phys. Chem. A, 101, 3125-3134, 1997.

IUPAC: IUPAC Subcommittee on Gas Kinetic Data Evaluation – Data Sheet HOx_VOC1, http://www.iupackinetic.ch.cam.ac.uk/index.html, updated 12. 12. 2007, (see also Atkinson et al., 2004), 2007.

Jöckel, P., Kerkweg, A., Pozzer, A., Sander, R., Tost, H., Riede, H., Baumgaertner, A., Gromov, S., and Kern, B.: Development cycle 2 of the Modular Earth Submodel System (MESSy2), Geosci. Model Dev., 3, 717-752, doi:10.5194/gmd-3-717-2010, 2010.

Keene, W. C., Sander, R., Pszenny, A. A. P., Vogt, R., Crutzen, P. J., and Galloway, J. N.: Aerosol pH in the marine boundary layer: A review and model evaluation, J. Aerosol Sci., 29, 339–356, doi:10.1016/S0021-8502(97)10011-8, 1998.

Sander, S. P., Barker, J. R., Golden, D. M., Kurylo, M. J., and Wine, P. H.: Chemical Kinetics and Photochemical Data for Use in Atmospheric Studies, Evaluation Number 17, JPL Publication 10-6, Jet Propulsion Laboratory, Pasadena, CA, 2011.